Liu *et al. Biochar* (2026) 8:86
https://doi.org/10.1007/s42773-026-00596-x

Biochar

ORIGINAL RESEARCH Open Access

Biochar-regulated transport of weakly hydrophobic antibiotics between macropore and matrix domains in structured soil

Xinyu Liu[1,2,3], Yang He[1,4,5*], Jinghan Li[1], Shijie Zheng[1], Lei Zhang[1], Jianqiang Zhang[1] and Xiangyu Tang[2,6]

Abstract

Biochar amendments show promise for mitigating accelerated antibiotic transport caused by macropore flow in soil, yet their effectiveness in such systems is poorly understood, lacking direct evidence differentiating biochar's role across macropore flow versus soil matrix infiltration. Using a novel macropore and matrix domains (dual-domain) separation apparatus, this study quantified the effect of biochar addition on the transport of weakly hydrophobic antibiotics, sulfadiazine (SDZ) and florfenicol (FFC), in soils under hydraulically isolated and connected domain conditions. Results suggested that biochar's efficacy is significantly amplified when hydraulic connectivity between the dual domains is present. In this state, it actively diverts antibiotics from macropore flow into the soil matrix infiltration, significantly reducing the total cumulative mass fluxes (CMFs) of SDZ from 0.72 ± 0.01 to 0.61 ± 0.00 and FFC from 0.81 ± 0.04 to 0.72 ± 0.02 ($p < 0.05$). Partial least squares structural equation modeling (PLS-SEM) subsequently revealed that biochar rewires the system's causal pathways. The model showed that it leverages mobile carriers (dissolved organic matter and colloids) to create a powerful immobilizing sink in the matrix, while counteracting the advective flux traced by Br^-. These findings support the new hypothesis that biochar functions as a dynamic "biochar sorption pump" (BSP). This framework reframes biochar from a passive sink to an active flux regulator, providing a basis for designing precision remediation strategies based on soil hydraulic properties to protect vulnerable aquatic ecosystems.

Highlights

- A novel apparatus physically separates the effluent from macropore and matrix domains for flux analysis.
- The "biochar sorption pump" (BSP) hypothesis is proposed and validated for contaminant regulation.
- Activation of the BSP depends on macropore and soil matrix hydraulic connectivity.
- Biochar is reframed from a passive sorbent to an active hydrological regulator of contaminant flux.

Keywords Weakly hydrophobic antibiotics, Macropore flow, Structured soil, Dual-domain, PLS-SEM, Biochar sorption pump

*Correspondence:
Yang He
yanghe@swjtu.edu.cn
Full list of author information is available at the end of the article

Springer

Graphical Abstract

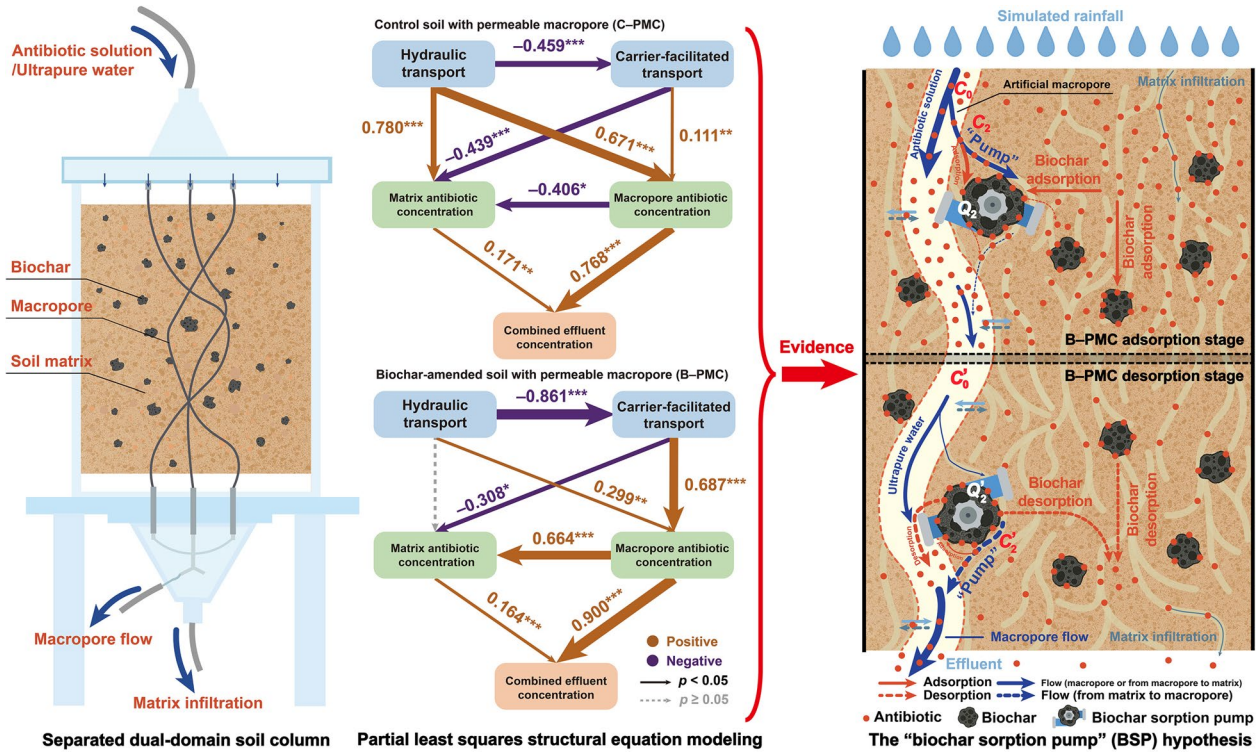

1 Introduction

Biochar is widely recognized as an effective soil amendment for immobilizing emerging contaminants and heavy metals, thereby mitigating their bioavailability and leaching risks (Liu et al. 2019a; Tang et al. 2024). However, its role in regulating weakly hydrophobic antibiotics is disputed and scale-dependent. At the column scale, uniform conditions highlight biochar's exceptional sorption capacity (He et al. 2019; Zou and Zheng 2013). This can increase the sorption distribution coefficient (K_d) for polar pesticides up to 2.4–2.5 times (Lei et al. 2020). Conversely, at the field scale, biochar's influence on soil hydraulic properties is critical, reducing vertical infiltration by 41–43% and altering runoff (Lu et al. 2023). These hydraulic alterations affect antibiotic-sorption site contact, increasing the risk of bypass flow around the biochar-amended matrix (Tang et al. 2024). This creates a conundrum in structured soils concerning how biochar sorption interacts with the macropores to determine real-world effectiveness (Li et al. 2020a). Furthermore, our prior research showed that field aging modifies biochar's kinetic retention capacity over time (Liu et al. 2025a), highlighting dynamic regulatory interactions beyond simple equilibrium sorption. This issue is pronounced in soils like purple soil, which is prone to macropore leaching, a key driver of non-point source pollution (Liu et al. 2019a; Tang et al. 2024). Consequently, these unresolved complexities hinder prediction and optimization of biochar performance in agricultural systems.

In structured soils, biochar's role extends beyond that of a simple sorbent to that of a physical soil conditioner that alters the dual-domain architecture (Li et al. 2024; McCarter et al. 2020). Techniques like X-ray micro-computed tomography (micro-CT) show that biochar modifies soil pore networks and aggregation, which is crucial for regulating water movement and mass exchange between the soil matrix and macropore (Yu et al. 2016). While structural macropores (0.1–5% of soil volume) typically dominate convective flux (ca. 90%), biochar embedded within the soil matrix can restructure these hydraulic dynamics by increasing intra-aggregate porosity (Cao et al. 2024). Our related research demonstrated that high flow velocities typical of macropores induce a dispersion-dominated regime where physical transport overrides chemical sorption (Zhang et al. 2025). This finding suggests that biochar's ability to modify the soil's physical structure and hydraulic properties at the macropore–matrix interface may be as important as its sorption capacity

in controlling contaminant fate. However, a critical gap remains in the literature: while biochar's hydraulic and sorption effects are well-documented separately, few studies have mechanistically coupled these processes in structured soils (Liu et al. 2025a; Tang et al. 2024). Conventional two-region models (TRM) obscure the true mechanisms at this critical interface by relying on empirically fitted coefficients (the mass transfer coefficient, α; mobile water fraction, f and K_d). This challenge is amplified by the inability of conventional columns to physically separate macropore flow and matrix infiltration (Li et al. 2020b). Consequently, the mechanisms of these coupling effects between biochar within the soil matrix and transport dominated by macropores remain speculative, lacking direct experimental evidence that differentiates flux contributions from each domain.

This leads to a fundamental uncertainty regarding the coupled mechanism by which biochar regulates water and contaminant transport in structured soils. It is unclear whether it acts as a passive sink, affecting only contaminant concentrations within the soil matrix, or as an active regulator that controls the contaminant flux partitioning between the two domains (Huan et al. 2024; Souza et al. 2024). To resolve this, this study investigates a novel coupled mechanism where biochar actively modulates contaminant exchange at the macropore–matrix interface. This study proposes that biochar embedded within the soil matrix creates a steep physicochemical potential gradient, actively partitioning contaminant flux from the macropore domain dominated by advection into the matrix domain, where transport is diffusion-limited, for sequestration (Jia et al. 2023; Miele et al. 2023). This effectively intercepts pollutants lost via preferential transport pathways. Previous studies inferred these mechanisms from integrated breakthrough curves (He et al. 2019; Zou and Zheng 2013). However, verifying the flux-partitioning mechanism is hindered by the inability of conventional methods to separately quantify solute fluxes from macropore and matrix domains (Dong et al. 2022).

To overcome this limitation, this study employed a novel apparatus to physically isolate and collect macropore flow and matrix infiltration, enabling direct quantitative analysis of how biochar regulates contaminant transport and partitioning. Therefore, this study aimed to (1) quantify field-aged biochar's differential impacts on antibiotic transport within the macropore and matrix domains and evaluate how macropore wall permeability governs this transport; (2) statistically interpret how biochar alters the causal pathways of antibiotic flux between macropore and matrix domains using both experimental data and partial least squares structural equation modeling (PLS-SEM); and (3) utilize these experimental and statistical insights to elucidate mechanisms of biochar's regulation of antibiotic transport within each domain. Ultimately, this work aimed to bridge contaminant-soil matrix interactions and dual-domain transport processes.

2 Material and methods

2.1 Materials and reagents

The biochar used in the experiments was pyrolyzed from a mixture of agricultural residues (comprising straw, stems, and haulms sourced from Sanli New Energy Co., Ltd.) at 500 °C. This pyrolysis temperature was selected to balance the development of porous structures with the retention of oxygen-containing functional groups, and to align with the standard industrial production parameters used for regional farmland restoration (Ivanova et al. 2023). Key physicochemical characteristics are detailed in the Supplementary Material (Table S1).

The weakly hydrophobic antibiotics sulfadiazine (SDZ) and florfenicol (FFC) (> 98% purity, Aladdin Technology Co., Ltd., Shanghai, China) were selected for this study, owing to their high detection frequency in local water bodies and their potential for preferential transport in structured soils (Hu et al. 2025). SDZ and FFC were selected to represent distinct physicochemical behaviors, specifically contrasting amphoteric with non-ionizable characteristics, to validate the transport regulatory mechanisms across different contaminant types. Their properties are provided in the Supplementary Material (Table S2). Analytical grade potassium bromide (KBr, Sinopharm Chemical Reagent Co., Ltd., Shanghai, China) served as a conservative tracer to delineate solute transport pathways. Crucially, Br^- established the hydraulic baseline as an internal control, while trace antibiotics exerted negligible physicochemical feedback on soil properties, ensuring transport deviations resulted exclusively from sorption interactions.

LC/MS-grade acetonitrile and methanol were purchased from Thermo Fisher Scientific (Waltham, MA, USA). Other analytical grade reagents, including $CaCl_2$, Na_2HPO_4, citric acid, and NaOH for pH adjustment, were obtained from Kelong Chemical Reagent Co., Ltd. (Chengdu, China). Ultrapure water from a Millipore Milli-Q system (Bedford, MA, USA) was used for all solution preparations.

2.2 Experimental design for dual-domain separation

To deconstruct the complex interplay between soil matrix infiltration and macropore flow observed in natural, undisturbed soils, this study employed an established experimental design using repacked soil columns with artificially constructed macropores (Text S1 and Figure S1). Unlike undisturbed soil cores, which were

left intact, the collected soil was air-dried, ground, and passed through a 2-mm sieve prior to packing. This preprocessing effectively homogenized the matrix domain and destroyed natural structural aggregates or root channels, thereby eliminating matrix-generated preferential flow and ensuring that the artificial macropores acted as the exclusive preferential pathways. Building upon our previous work identifying the macropore flow as a critical pathway for antibiotic transport, columns were constructed from calcareous purple soil collected in 2019 (Liu et al. 2025a) from a long-term experimental site (established in 2014) in Yanting County (105°27′E, 31°19′N), China. Specifically, biochar-amended treatments contained field-aged soil collected from the 1% (w/w) biochar-amended plots (aged 5 years; see Text S2 for field history and environmental conditions), while control columns used unamended soil from adjacent plots. All collected soil samples were air-dried, ground, and passed through a 2-mm sieve to ensure homogeneity. This soil features well-developed macropores known to exhibit significant preferential transport in the region (Xian et al. 2018).

This study investigated four macropore soil column treatments using a purple soil, whose physicochemical properties are detailed in Table 1. The treatments combined control (C) and biochar-amended (B) soils with either impermeable (IMC) or permeable (PMC) macropores, creating four distinct setups: C–IMC, C–PMC, B–IMC, and B–PMC. This factorial design decoupled hydraulic connectivity from sorption, where IMC assessed passive limits under physical isolation and PMC verified the active flux regulation mechanism enabled by connectivity. Each column, prepared in triplicate, contained three spirally wound artificial macropores (30-cm length, 3-mm inner diameter) simulating natural tortuosity engineered to statistically replicate natural characteristics (porosity ca. 0.46; Figure S1, Table S3).

Table 1 Basic physicochemical properties of the purple soils

Property	Control soil (C)	Biochar-amended soil (B)	Unit
Soil organic carbon (SOC)	17.43 ± 0.55	35.85 ± 0.21	g kg^{-1}
Total nitrogen (TN)	0.82 ± 0.10	1.11 ± 0.01	g kg^{-1}
Cation exchange capacity (CEC)	10.90 ± 1.27	13.53 ± 0.09	$cmol^{+}$ kg^{-1}
pH	8.29 ± 0.03	7.82 ± 0.00	–
Texture (Clay)	11.1	10.9	%
Texture (Silt)	49.74	43.34	%
Texture (Sand)	39.16	45.76	%
Soil type	Loam	Loam	–

Impermeable macropores used flexible silicone tubing; permeable ones used porous fiberglass sleeving to permit inter-domain exchange (Manns et al. 2024; Urbina et al. 2019). These materials were selected based on established methods for structural stability, comparable hydraulic conductivity, and negligible antibiotic adsorption, minimizing experimental artifacts (Zhang et al. 2025) (Text S3, Tables S4 and S5). Biochar amendment resulted in lower bulk densities and higher porosities than control columns, with similar pore flow velocities across setups (Table S5).

A novel patented apparatus was employed (He et al. 2022), featuring a main soil column cylinder (14-cm inner diameter) where a peristaltic pump delivers influent via a top-mounted distributor (Fig. 1). The key innovation is a specialized base collector. A perforated plate supports the soil matrix, while separate conduits channel the macropore flow into a dual-domain separation collector. This collector uses a flow splitter to physically separate the macropore flow and matrix infiltration, enabling discrete quantification of water and solute fluxes from each domain.

To strictly control the soil porosity, a mass-volume control method was employed rather than post-packing measurements (Zou and Zheng 2013). Soil columns were wet-packed to 13 cm using precise pre-weighed masses calculated from the soil particle density to ensure target bulk density and homogeneity. Control columns used unamended soil from adjacent plots processed identically. For uniform influent distribution and drainage, 2-cm layers of quartz sand (particle size ca. 2.5–3.5 mm) were placed at the top and bottom of each column, respectively.

2.3 Column experiments and solute transport analysis

Each soil column was first pre-conditioned with 2–3 pore volumes (PV) of a 0.01 mol L^{-1} $CaCl_2$ background solution to establish hydrochemical equilibrium and steady-state transport conditions. Subsequently, a 4 PV pulse containing 50 mg L^{-1} Br^{-} (conservative tracer), 1.0 mg L^{-1} SDZ and FFC was applied using a peristaltic pump at a constant flow rate. This concentration simulates a high-input agricultural scenario, ensuring both environmental relevance and reliable analytical quantification (Zou and Zheng 2013). An immediate 4 PV flushing stage using $CaCl_2$ solution followed to assess desorption. The 8 PV duration was selected based on pre-experiments to ensure complete breakthrough and subsequent elution to near-zero concentrations. Degradation was considered negligible due to the short hydraulic residence time relative to reported half-lives (Engelhardt et al. 2015; Zou and Zheng 2013). The PV was calculated based on the total

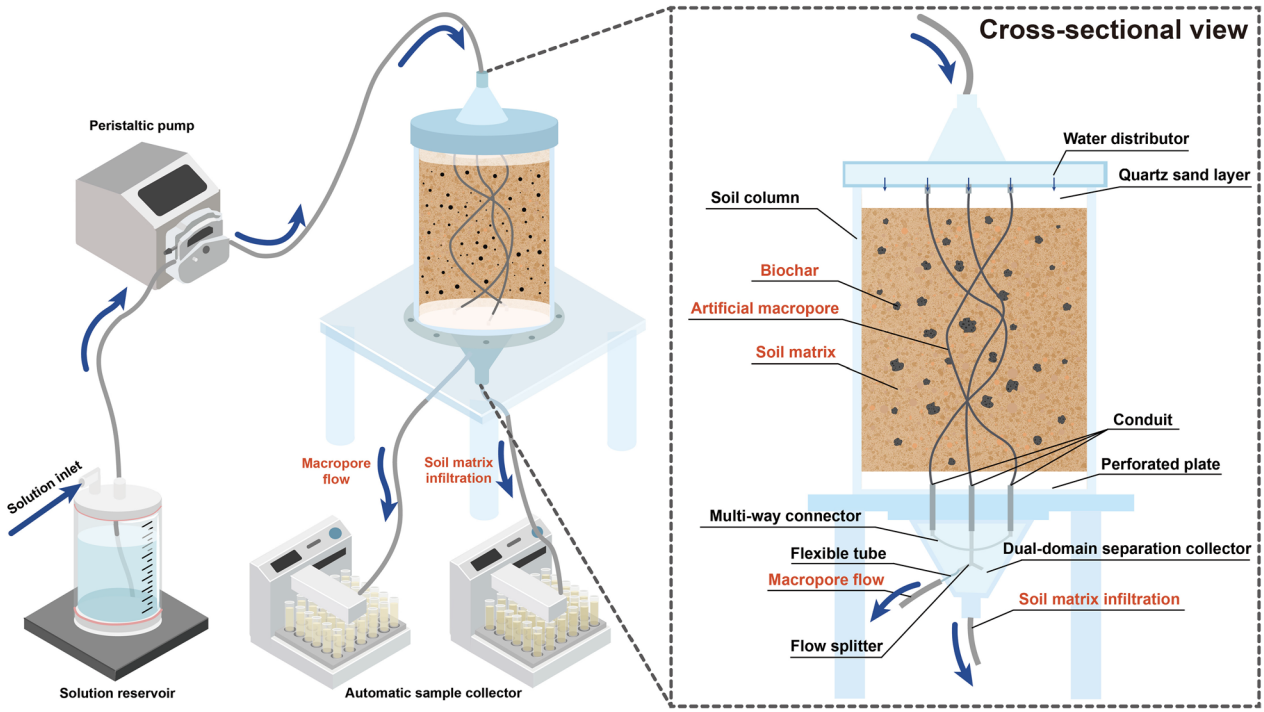

Fig. 1 Schematic of the setup for separated dual-domain soil column experiment

effective porosity (macropore plus matrix) to maintain a unified baseline. Throughout the 8 PV experiment, macropore flow and matrix infiltration were collected separately and simultaneously, with combined effluent also gathered for comparison. All samples were stored at 4 °C and analyzed within 24 h. Breakthrough curves (BTCs) were generated by plotting the relative effluent concentration (C/C_0) versus cumulative PV. All column experiments were conducted in triplicate to ensure reproducibility.

Concentrations of SDZ and FFC were quantified using high-performance liquid chromatography (HPLC) (Liu et al. 2025b). Effluent pH and electrical conductivity (EC) were measured using standard methods (Liu et al. 2025c), while Br^- concentrations were measured with an ion-selective electrode. Dissolved organic carbon (DOC) and colloid levels were quantified via UV spectrophotometry (Liu et al. 2024). Additional details regarding analytical procedures and quality control are provided in the Text S4.

2.4 Modeling and statistical analysis

Antibiotic mass fluxes from the matrix domain, macropore domain, or combined dual-domain were calculated from measured concentrations and flow rates. To evaluate biochar's retention, the mass recovery rate was calculated as the percentage of total eluted relative to input mass, quantifying cumulative export and retention efficiency. Hydrus 1D (v. 4.17.0140, PC-Progress) simulated solute transport and fit BTCs. The convection–dispersion equation (CDE) was applied for single-domain transport conditions. A TRM assuming physical non-equilibrium conceptualized the two domains. The TRM partitions the soil porous medium into a mobile macropore domain and a less mobile matrix domain, with solute exchange governed by a first-order mass transfer coefficient (α). Key equations are provided in the Supplementary Material (Text S5 and Eqs. S1–S3).

The causal network of antibiotic transport was analyzed using PLS-SEM with SmartPLS (v4.1.1.2) (Hair and Sabol 2025). Model evaluation involved two stages. First, the measurement model's reliability (Cronbach's alpha and composite reliability > 0.8) and convergent validity (AVE > 0.5) were confirmed. Second, the structural model was assessed by examining path coefficient significance via bootstrapping (5,000 resamples) and ensuring overall goodness-of-fit (GoF) exceeded 0.36 (Wang 2025). Collinearity among latent variables was examined using the Variance Inflation Factor (VIF). All Inner VIF values were below the maximum threshold of 10 (Mason and Perreault 1991). Additional calculation formulas and evaluation criteria are in Text S6. Descriptive statistics used SPSS

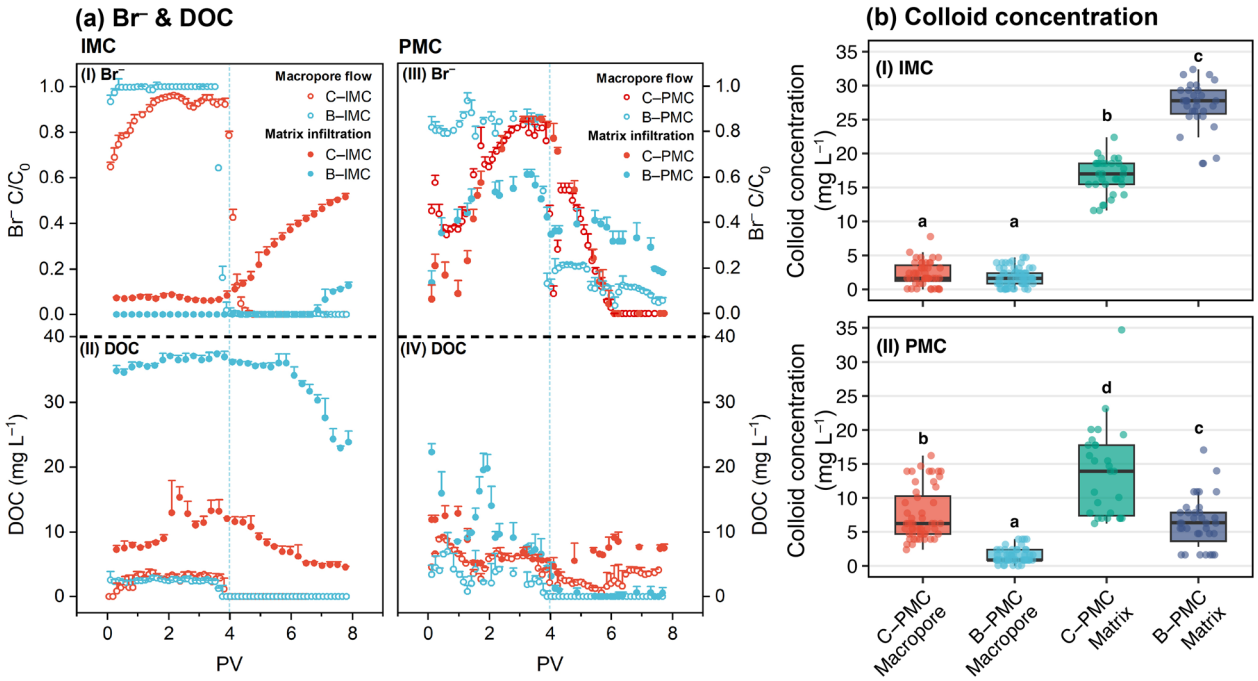

Fig. 2 Hydrodynamic and hydrochemical responses in dual-domain soil columns, showing Br^- breakthrough, dissolved organic matter (as DOC) (**a**) and colloid concentration (**b**) from macropore flow and matrix infiltration under control (C) and biochar treatments (B) with impermeable (IMC) and permeable (PMC) macropores

26.0 with a significance level of $p < 0.05$, and figures were generated with Origin 2021 and R 4.3.0.

3 Results

3.1 Hydrodynamic and hydrochemical conditions in the dual domains

To elucidate the fundamental transport processes governing solute behavior, the transport and hydrochemical conditions in the separated macropore and matrix domains were examined first. Solute transport, traced by Br^- (Fig. 2aI, III), confirmed the successful physical separation of the two domains by the apparatus. Across all treatments, Br^- BTCs from the macropore flow were characterized by rapid arrival and high peak concentrations, whereas the matrix infiltration showed significantly delayed and attenuated responses. For instance, in the permeable C–PMC column, Br^- in the macropore flow reached $C/C_0 > 0.5$ within the first 0.5 PV, while the matrix infiltration required nearly 4 PV to reach a similar level. Biochar amendment (B–PMC) appeared to increase tailing in the macropore flow and slightly accelerated the tracer's appearance in the matrix infiltration, suggesting subtle alterations to transport pathways. These distinct BTCs validate that macropore flow constitutes a rapid transport pathway while the matrix infiltration is characterized by a much slower transport pathway. Given that Br^- is a conservative tracer, its behavior directly reflects the advective flux within each domain and was retained as a key explanatory variable in the subsequent SEM analysis.

The effluent pH and EC were monitored to provide an overall hydrochemical context (Figure S2). Effluent pH remained slightly alkaline (ranging from 7.2 to 8.4), consistent with the calcareous nature of the purple soil, while EC values, peaking at approximately 1800 μS cm^{-1} in the macropore flow, closely mirrored the Br^- tracer profiles. Importantly, while minor fluctuations were observed, neither macropore permeability nor biochar amendment caused major shifts in the overall pH and EC patterns that could be directly correlated with the substantial changes in antibiotic fate. Consequently, they were excluded from the final PLS-SEM analysis to achieve a more parsimonious model. Furthermore, the stable EC profile implies that ionic effects were subordinate to the dominant hydrophobic partitioning and hydraulic forces governing antibiotic transport.

The release of dissolved organic matter (DOM), quantified via dissolved organic carbon (DOC) concentrations, was strongly influenced by macropore, soil matrix and biochar (Fig. 2aII, IV). In control columns (C–IMC and C–PMC), DOC concentrations were consistently low, typically remaining below 10 mg L^{-1} in both domains. In contrast, biochar amendment significantly increased DOC release, an effect almost exclusively confined to the

matrix domain. In the B–IMC treatment, DOC concentrations of matrix infiltration peaked at nearly 40 mg L^{-1}, approximately four times higher than in the C–IMC matrix infiltration. Conversely, DOC levels in the B–PMC macropore flow remained low and comparable to the C–PMC, demonstrating that biochar primarily modifies the hydrochemistry of soil matrix.

Colloid release showed distinct trends dependent on interface properties between the domains (Fig. 2b). In the IMC treatment, biochar amendment significantly increased colloid concentrations, likely driven by the release of fine biochar particles and dispersion of soil colloids within the confined matrix. The median concentration in B–IMC matrix infiltration (ca. 28 mg L^{-1}) was approximately 1.5-fold higher than that in the C–IMC matrix infiltration and over fivefold higher than the corresponding macropore flow. In stark contrast, in the PMC treatment, biochar reduced colloid release, with median concentrations in both matrix infiltration (ca. 7 mg L^{-1}) and macropore flow (ca. 4 mg L^{-1}) lower than those in the C–PMC treatment. This reduction indicates that the permeable interface promoted physical straining and re-deposition, effectively filtering mobile colloids. Although biochar-derived colloids responded variedly to interface permeability, their release occurred primarily within the matrix domain, where transport is slower. Thus, their potential as a significant vector for inter-domain antibiotic transport was considered secondary to dissolved-phase interactions.

3.2 Antibiotic transport and partitioning

The transport and partitioning of SDZ and FFC between the separated macropore and matrix domains were evaluated via breakthrough curves (BTCs) and cumulative mass fluxes (CMFs) (Fig. 3, Table S6). In control columns, the permeability of the macropore wall was the determining factor. For C–IMC, where the domains were isolated, the antibiotic mass flux was overwhelmingly dominated by the macropore flow, which rapidly reached high C/C_0 plateaus (SDZ ≈ 0.92, FFC ≈ 1.00) within 2 PV (Fig. 3aI, II). In contrast, the matrix infiltration showed minimal, delayed breakthrough (SDZ C/C_0 reached only 0.3 at 8 PV). During the desorption stage (4–8 PV), antibiotic concentrations in the macropore flow dropped sharply while the matrix infiltration showed a slow, sustained release. Consequently, after 8 PV, the relative maximum CMFs for SDZ and FFC in the macropore flow were 0.78 ± 0.02 and 0.85 ± 0.02, respectively, while matrix contributions were negligible (Fig. 3bI, II). Conversely, in C–PMC, permeable walls enabled significant inter-domain exchange between the two domains. The matrix infiltration exhibited substantial and earlier breakthrough, with peak C/C_0 values of approximately 0.82 for SDZ and 0.90 for FFC (Fig. 3aIII, IV). This was reflected in the CMFs, where the flux contribution from the matrix infiltration increased to 0.19 ± 0.00 for SDZ and 0.21 ± 0.02 for FFC, with macropore flow contributing 0.53 ± 0.01 and 0.60 ± 0.02, respectively (Fig. 3bIII, IV).

Biochar amendment markedly influenced antibiotic BTCs and mass flux partitioning, particularly when the

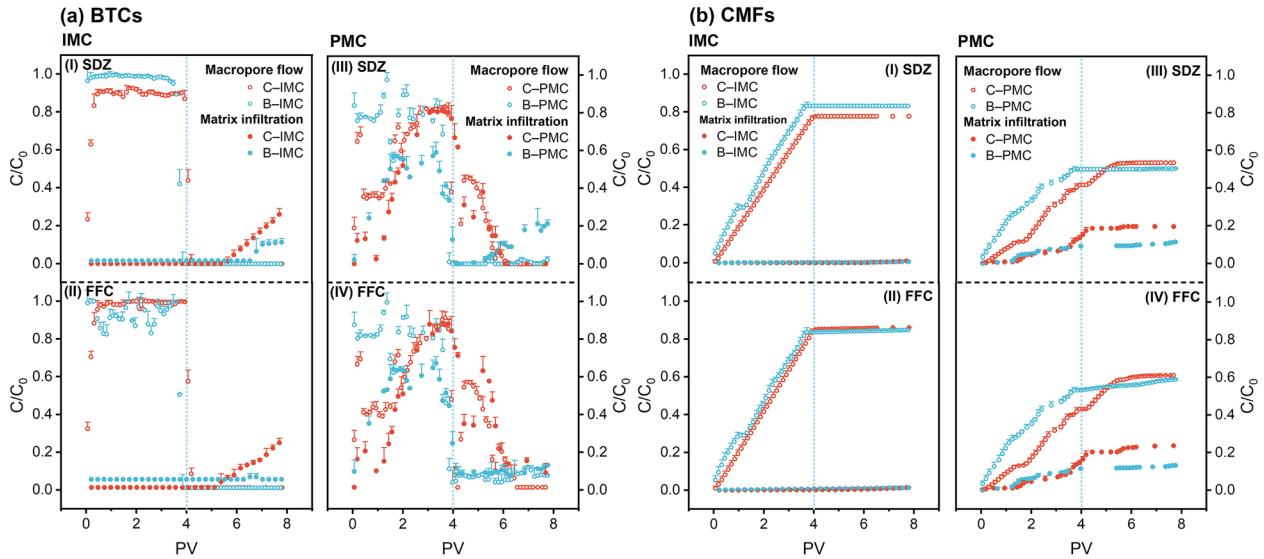

Fig. 3 Breakthrough curves (BTCs) and cumulative mass fluxes (CMFs) of sulfadiazine (SDZ) and florfenicol (FFC) in macropore flow and matrix infiltration from dual-domain soil columns, illustrating transport under control (C–) and biochar treatments (B–) with impermeable (IMC) (**a**) and permeable (PMC) (**b**) macropores

interface between the macropore and matrix domains was permeable. In the B–IMC treatment, CMF profiles were nearly identical to C–IMC, indicating biochar's effectiveness is severely limited without hydraulic connectivity between the domains. In stark contrast, the B–PMC treatment showed the most profound effects, with biochar addition leading to lower peak C/C_0 values and greater retardation in both domains. This enhanced sequestration was most evident in the CMFs (Fig. 3bIII, IV). For SDZ, the total relative maximum CMF (macropore and matrix) decreased from 0.72 ± 0.01 in C–PMC to 0.61 ± 0.00 in B–PMC ($p < 0.05$). This reduction resulted from decreases in both macropore flow (0.53 ± 0.01 to 0.50 ± 0.00) and matrix infiltration (0.19 ± 0.00 to 0.11 ± 0.00). Similarly, for FFC, the total relative maximum CMF dropped from 0.81 ± 0.04 to 0.72 ± 0.02 ($p < 0.05$), driven by decreases in macropore flow (0.60 ± 0.02 to 0.59 ± 0.01) and matrix infiltration (0.21 ± 0.02 to 0.13 ± 0.01). These quantitative differences demonstrate that biochar's ability to enhance antibiotic sequestration is primarily activated by hydraulic connectivity between the domains.

3.3 Analysis of combined effluent and transport modeling

Following the detailed analysis of the separated dual-domain, the combined effluent was analyzed to provide a system-level baseline and for quantitative model fitting. This integrated output represents the total flux from both the macropore and matrix domains and is typical of conventional column studies (Zou and Zheng 2013). BTCs for the conservative tracer (Br^-) and the two antibiotics in the combined effluent are shown in Fig. 4. For Br^-, all columns exhibited early breakthrough and significant tailing, a feature particularly pronounced in columns with permeable macropores (PMC) compared to those with impermeable ones (IMC) (Fig. 4a, d). In the PMC columns, the peak relative concentration (C/C_0) of Br^- was approximately 0.9 with broad tailing, whereas in the IMC columns, it formed a sharper plateau near 1.0, reflecting the different levels of interaction between the two domains. These asymmetrical BTCs are characteristic of dual-domain transport (Pollacco et al. 2024).

The antibiotic BTCs also indicated reactive, non-equilibrium transport, with pronounced tailing and significant retardation relative to Br^- (Fig. 4b, c, e, f). In control columns, FFC generally showed slightly earlier breakthrough and higher peak concentrations than SDZ. The addition of biochar consistently resulted in greater retardation and lower peak effluent concentrations for both antibiotics. This overall reduction in antibiotic mass flux was quantified in the PMC, where the peak C/C_0 for SDZ decreased from 0.85 (C–PMC) to 0.75 (B–PMC), and

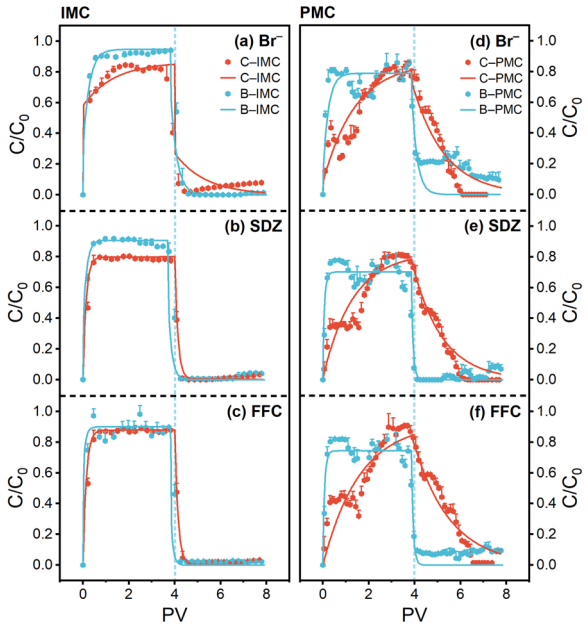

Fig. 4 Breakthrough curves (BTCs) showing experimental data (points) and corresponding the convection-dispersion equation (CDE) and two-region models (TRM) model fits (solid lines) for bromide (Br^-), sulfadiazine (SDZ), and florfenicol (FFC) in combined effluent from impermeable (IMC) and permeable (PMC) macropore soil columns under control (C–) and biochar-amended (B–) conditions

for FFC from 0.88 to 0.78 (Fig. 4e, f). These observations demonstrate that biochar reduces the total antibiotic flux at the column scale, but the underlying mechanism requires further deconvolution.

To deconvolve the underlying mechanisms, the BTCs were successfully simulated using the CDE (Br^-) and TRM for SDZ and FFC within Hydrus 1D (Table 2). The Br^- fitting parameters provided insights into the inter-domain exchange between the two domains. Compared to IMC, PMC consistently exhibited higher hydrodynamic dispersion (D) and α value, alongside a lower f value. Notably, the α value, a critical indicator of inter-domain exchange, increased fivefold from 0.04 min^{-1} in C–IMC to 0.20 min^{-1} in C–PMC, and was further enhanced by biochar to a maximum of 0.65 min^{-1} in B–PMC. For the antibiotics, the TRM fitting revealed that the α value, negligible in the C–IMC treatment, reached its maximum in the B–PMC treatment (SDZ: 0.86 min^{-1}; FFC: 1.03 min^{-1}). This provides strong, model-derived evidence that biochar in a system with connected domains enhances solute mass transfer from the macropore domain into the matrix domain. Furthermore, the K_d values were generally higher for FFC than SDZ, and biochar substantially increased K_d for both antibiotics, particularly for FFC in the B–PMC treatment

Table 2 Fitting parameters of SDZ and FFC in soil columns

Test soil column	Antibiotic	V (cm h^{-1})	D (cm^2 h^{-1})	λ (cm)	f	α (h^{-1})	K_d (L kg^{-1})	R^2	RMSE
C–IMC	Br^-	1.12	63.56	56.86	0.46	0.04	–	0.96	0.08
	SDZ	1.12	63.56	56.86	0.46	0.00	0.10	0.99	0.04
	FFC	1.12	63.56	56.86	0.46	0.00	0.20	0.99	0.04
C–PMC	Br^-	1.12	114.90	102.56	0.36	0.20	–	0.90	0.04
	SDZ	1.12	114.90	102.56	0.36	0.47	0.11	0.92	0.04
	FFC	1.12	114.90	102.56	0.36	0.54	0.20	0.88	0.05
B–IMC	Br^-	1.16	102.11	88.41	0.47	0.45	–	0.83	0.19
	SDZ	1.16	102.11	88.41	0.47	0.54	0.12	0.84	0.07
	FFC	1.16	102.11	88.41	0.47	0.58	0.28	0.86	0.09
B–PMC	Br^-	1.13	145.33	129.06	0.32	0.65	–	0.91	0.15
	SDZ	1.13	145.33	129.06	0.32	0.86	0.14	0.98	0.06
	FFC	1.13	145.33	129.06	0.32	1.03	0.28	0.92	0.08

V, average pore water velocity (cm h^{-1}); D, hydrodynamic dispersion coefficient (cm^2 h^{-1}); λ, dispersivity (cm); f, fraction of equilibrium sorption sites (dimensionless); α, first-order kinetic mass transfer coefficient (h^{-1}); K_d linear distribution coefficient (L kg^{-1}); R^2, coefficient of determination; RMSE, root mean square error

(from 0.20 to 0.28 L kg^{-1}), indicating stronger sorption. The goodness-of-fit statistics confirm the TRM's applicability, and these model-derived parameters, especially the significant increase in α value, provide strong quantitative evidence that biochar actively enhances mass transfer from the macropore domain to the matrix domain, even when analyzing the integrated effluent.

4 Discussion

4.1 Impact of macropore wall permeability on solute transport

Macropore wall permeability was a decisive factor governing the hydraulic connectivity and solute exchange between the macropore and matrix domains. In C–IMC, the channels functioned as discrete, rapid bypass conduits, largely isolating the rapid macropore flow from the slower matrix infiltration (Fig. 5a). This segregation was evident in the tracer (Br^-) and antibiotic BTCs, which showed sharp, early peaks in macropore flow but severely delayed signals from the matrix infiltration (Fig. 3I, III). Consequently, antibiotic transport in C–IMC was overwhelmingly channeled through these impermeable macropores, leading to rapid elution with minimal opportunity for solute transfer into the matrix infiltration (Fig. 4). This aligns with studies identifying macropore flow as a critical process for contaminant leaching (Jiang et al. 2023). This limited interaction curtails the soil's natural attenuation capacity (Souza et al. 2024) and exemplifies the mobile–immobile region phenomenon (Li et al. 2020b), where restricted exchange with the soil matrix maximizes contaminant leaching risk (Jia et al. 2023).

Conversely, permeable macropore walls substantially enhanced the hydraulic and solute exchange between the two domains (Fig. 5b), as confirmed by the earlier, more significant tracer breakthrough in the PMC matrix domain (Fig. 3I, III). This lateral exchange is crucial as it offers a route for pollutants in macropore flow to reach the larger volume of matrix infiltration, where longer residence times allow for greater attenuation. Consequently, even without biochar, a significantly larger fraction of the antibiotic mass flux was transferred to and attenuated within the matrix domain, as reflected by more pronounced retardation in the BTCs (Fig. 4d). The increased interaction in C–PMC, driven by active matrix diffusion and lateral advective–dispersive exchange (Miele et al. 2023), allowed the soil matrix domain to better buffer the contaminant pulse, confirming that macropore–matrix interface properties are key determinants of solute attenuation in such soils (Du et al. 2023).

Therefore, the treatments with impermeable and permeable interfaces represent two distinct transport regimes. The C–IMC treatment resembled a dual-porosity model, where the independent macropore network severely restricts the transfer of contaminants from the macropore into the soil matrix, neutralizing the matrix's potential for attenuation due to poor hydraulic connectivity. This aligns with previous work where a shift to dispersion-dominated transport at higher velocities overrode solute chemical properties (Zhang et al. 2025). The C–PMC treatment, however, behaved as a dual-permeability model with significant lateral exchange. This enhanced interaction fundamentally alters the transport regime, enabling the matrix domain to function as an effective sink, attenuating the solute flux transferred from the macropore domain. The degree of this exchange, and thus the overall attenuation of the antibiotic flux, is clearly a function of this wall permeability (Li et al. 2020a). Consequently, understanding

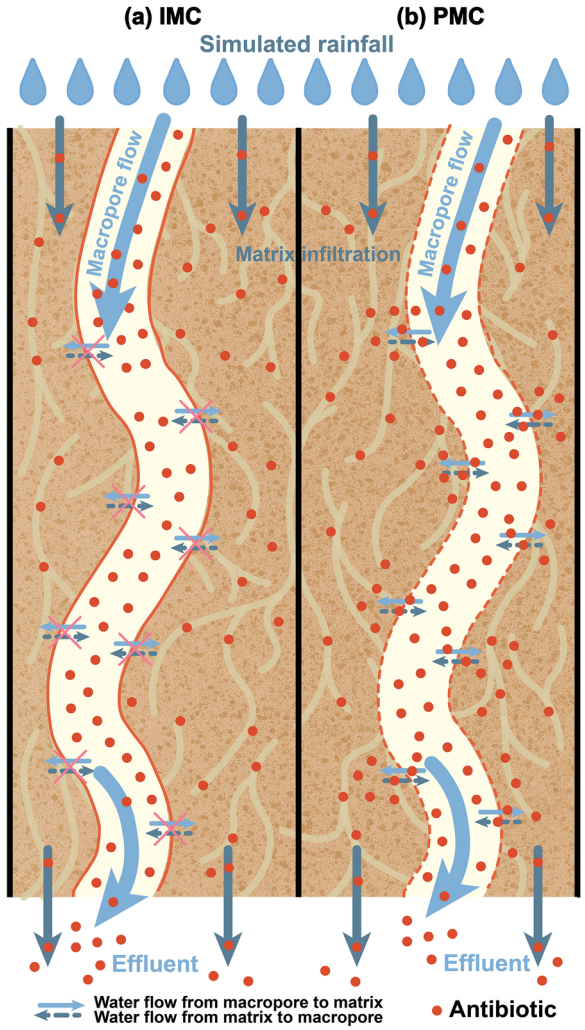

Fig. 5 Conceptual illustration contrasting the influence of macropore wall permeability on dual-domain solute transport mechanisms within biochar-amended soil columns featuring an impermeable macropore (IMC) and a permeable macropore (PMC)

these interface properties is essential for predicting contaminant transport and designing effective in situ remediation strategies (Souza et al. 2024). Although repacked columns represent a simplified model lacking natural aggregates, this trade-off was essential to mechanistically isolate macropore wall permeability. This design ensures reproducible hydraulic boundaries and strict domain decoupling unattainable in undisturbed soil cores (Silva et al. 2016; Zhang et al. 2025).

4.2 Deconstructing causal pathways of antibiotic flux with PLS-SEM

To quantitatively deconstruct governing mechanisms and differentiate the roles of advection, carrier-facilitation, and inter-domain exchange, this study employed PLS-SEM to test the causal network governing antibiotic transport in the dual-domain system (Hou et al. 2025; Lin 2022). The latent variables were defined by their respective manifest variables, such that hydraulic transport was measured by Br^- and Flux, while carrier-facilitated transport was measured by DOC and colloids, and both matrix and macropore antibiotic concentrations were measured by SDZ and FFC concentrations within their respective domains. Crucially, a direct causal path between the two domains was only tested in the permeable columns (PMC), as no physical mechanism for interaction exists in impermeable treatments (IMC). The final PLS-SEM results mapped the direct and indirect pathways influencing the combined effluent concentration under the four treatments (Fig. 6). A key finding across all models was the consistent, strong negative influence of hydraulic transport on carrier-facilitated transport (path coefficients from –0.459 to –0.906), a phenomenon attributed to a dilution effect where higher fluxes reduce DOC and colloid concentrations.

Analysis of control columns established a baseline for interface permeability effects. In C–IMC (Fig. 6a), with isolated domains, hydraulic transport was the primary driver for antibiotic movement, strongly influencing both matrix (path coefficient = 0.914) and macropore (0.892) concentrations, indicating advection dominance. Consequently, the final effluent was overwhelmingly determined by the macropore flow, evidenced by the extremely strong, positive path from macropore antibiotic concentration to combined effluent concentration (0.953), with only a minimal contribution from the matrix infiltration (0.159). Conversely, permeability in C–PMC (Fig. 6b) shifted system dynamics. Notably, the model revealed a significant negative path from macropore to matrix concentration (–0.406), reflecting a competitive transport regime where rapid macropore bypass diverts the majority of the solute flux, thereby restricting the mass available for matrix infiltration. Consequently, the macropore flow's influence on the final effluent, though still dominant, notably decreased (path coefficient = 0.768), while the matrix infiltration's contribution increased (0.171). This comparison confirms that a hydraulic connectivity is prerequisite for greater inter-domain interaction (Radolinski et al. 2021).

The introduction of biochar rewired these transport pathways. In the B–IMC treatment (Fig. 6c), with isolated domains, biochar's role was confined to a passive sink. This was evidenced by the strong negative path from carrier-facilitated transport to matrix antibiotic concentration (–0.861), reflecting localized sorption. However, domain isolation prevented influence on the macropore flow, so the final effluent was almost exclusively

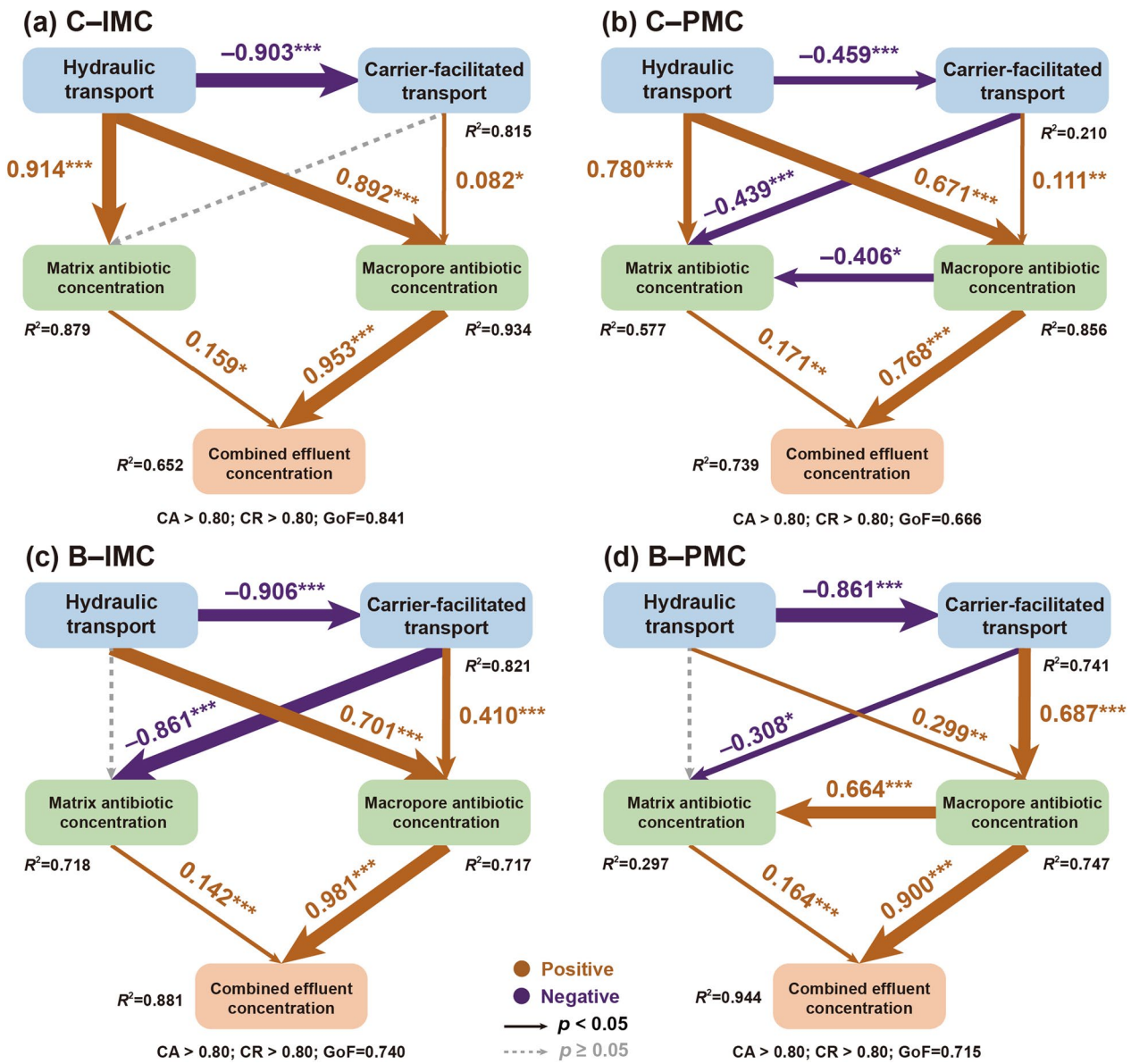

Fig. 6 Partial least squares structural equation models (PLS-SEM) illustrating the effects of biochar and macropore permeability on antibiotic transport pathways in (**a**) C–IMC, (**b**) C–PMC, (**c**) B–IMC, and (**d**) B–PMC treatments. Numbers represent standardized path coefficients (*, $p < 0.05$; **, $p < 0.01$; ***, $p < 0.001$). Dashed arrows indicate non-significant paths. R^2 values indicate variance explained for each dependent latent variable. Detailed summary of total effects on the combined effluent concentration and the collinearity assessment statistics (Inner VIF values) are provided in the Supplementary Material (Figure S3, Text S7, Table S7)

determined by macropore antibiotic concentration (path coefficient = 0.981). In stark contrast, a fundamental shift occurred in B–PMC (Fig. 6d). Here, active regulation was shown by the strong negative path from Carrier-facilitated transport to Matrix antibiotic concentration (–0.308) (Li et al. 2018; Liu et al. 2019b). Coupled with hydraulic connectivity, this strong sorption capacity fundamentally altered the inter-domain relationship. Crucially, the path from macropore to matrix concentration became strongly positive (0.664). This path reversal signifies a transition to sorption-driven source-sink dynamics. Specifically, biochar maintains a steep concentration gradient that drives active lateral mass transfer from the macropore into the matrix, effectively establishing a solute exchange bridge between the two domains. Furthermore, biochar dramatically enhanced the effect of carrier-facilitated transport on macropore antibiotic concentration (path coefficient = 0.687 vs. 0.111), suggesting

a dual role for biochar-derived mobile phases, consistent with known biochar–DOM interactions (He et al. 2019).

Ultimately, the PLS-SEM results offer robust quantitative insights into transport processes by explaining system-level outcomes via causal pathways. The models clearly distinguish between a passive sink (B–IMC) and an active, sorption-driven mechanism (B-PMC). Path coefficient analysis quantitatively explains experimental data, showing that biochar fundamentally alters the roles of hydraulic and carrier-facilitated transport. Specifically, biochar transforms carrier-facilitated transport into a powerful matrix immobilizer and simultaneously promotes macropore flow. The models also demonstrate a definitive shift from transport competition to sorption-regulated inter-domain exchange. This statistical evidence strongly supports a new mechanistic framework for biochar's role.

4.3 Biochar as a regulator of antibiotic flux partitioning

Dual-domain experimental data (Fig. 3) and causal pathways from PLS-SEM (Fig. 6) provide direct evidence for biochar's role as an active regulator of contaminant flux. In the IMC treatment, lacking hydraulic connectivity, antibiotic transport mirrored the Br^- and was confined to the macropore flow, carrying over 0.78 of the relative maximum CMF (Table S6). Biochar within the soil matrix had negligible impact, confirming ineffectiveness when bypassed by macropore flow (Zhang et al. 2025). Conversely, in the PMC treatment, biochar fundamentally altered the contaminant flux dynamics. It curtailed fluxes from both macropore and matrix outputs. Consequently, the total relative maximum CMF (macropore and matrix) significantly decreased from 0.72 ± 0.01 to 0.61 ± 0.00 for SDZ and from 0.81 ± 0.04 to 0.72 ± 0.02 for FFC ($p < 0.05$). This observation, along with the statistically identified shift to a source-sink dynamic, support the conceptualization of a "biochar sorption pump" (BSP) (Fig. 7). This hypothesis is conceptually analogous to established biogeochemical pump theories (Jiao et al. 2024; Liang et al. 2017; Chen et al. 2024). Here, the BSP describes a rapid, abiotic, sorption-driven physical process where biochar actively partitions the contaminant flux, driving it from the macropore domain into the matrix domain (Liu et al. 2022; Tang et al. 2024).

The BSP mechanism is conceptually sound within a dual-domain framework, which conceptualizes the soil porous medium as existing in two distinct yet interacting domains (Jia et al. 2023). Through rapid adsorption, biochar maintains a low aqueous concentration at the boundary, establishing a steep physicochemical potential gradient at the macropore–matrix interface. During the adsorption stage (0–4 PV), biochar's high sorption capacity significantly alters the local solid–liquid equilibrium (Q_2), maintaining low aqueous antibiotic concentrations (C_2) (Li et al. 2020a). This action establishes a steep concentration gradient between the influent (C_0) in the macropore flow and the low aqueous concentration (C_2) within the matrix infiltration. Consequently, biochar located deep within the matrix remains hydraulically isolated from the preferential flow, confirming that the BSP effect is exclusively localized at the active exchange interface. This gradient creates a powerful driving force for inter-domain mass transfer that activates the pump (Fig. 4b), analogous to reactive sinks in contaminant transport (Li et al. 2018; Sharma et al. 2021). Furthermore, the pump's efficacy is magnified by biochar's strong desorption hysteresis (4–8 PV), which locks captured antibiotics within the matrix, preventing their rapid release during subsequent flushing. This mechanism proved robust, operating effectively even with competing mobile components like DOM and colloids (Fig. 3). As the system approaches equilibrium, this net pumping effect attenuates, with the final sequestration capacity governed by both biochar's intrinsic properties and the hydraulic connectivity between the two domains.

This experimental approach and its findings advance our understanding beyond that provided by previous studies. While research using artificial macropores has been critical for quantifying mass transfer in structured soils, these studies have largely focused on hydraulic and tracer exchange, or used inert materials (Huan et al. 2024; Radolinski et al. 2021). The novelty here lies in incorporating an active amendment (biochar) into dual-domain to probe its effect on contaminant fluxes. This approach moves beyond simply parameterizing mass transfer with α values. By presenting evidence of macropore flow and matrix infiltration fluxes, it enables the deconstruction of why this transfer is enhanced, uncovering a robust sorption-driven regulatory mechanism.

In synthesis, the BSP hypothesis serves as a pivotal conceptual framework to reconcile the disconnect between column studies focused on sorption kinetics (He et al. 2019; Srinivasan and Sarmah 2015) and those dominated by field-scale transport processes (Tang et al. 2024). It demonstrates how a column-scale chemical property (biochar's intense sorption capacity) can exert direct control over a field-scale physical process (the inter-domain flux of contaminants) if the hydraulic prerequisite of a permeable interface is met. This integration of sorption chemistry and soil transport physics redefines biochar from a passive sink to a dynamic regulator of contaminant transport. This macroscopic partitioning extends established molecular mechanisms (pore filling, π–π interactions) (He et al. 2019; Liu et al. 2025a), demonstrating how hydraulic connectivity activates these micro-scale forces to drive inter-domain mass transfer. Furthermore, the porous structure of biochar provides habitats for soil microorganisms, fostering synergistic adsorption-biodegradation

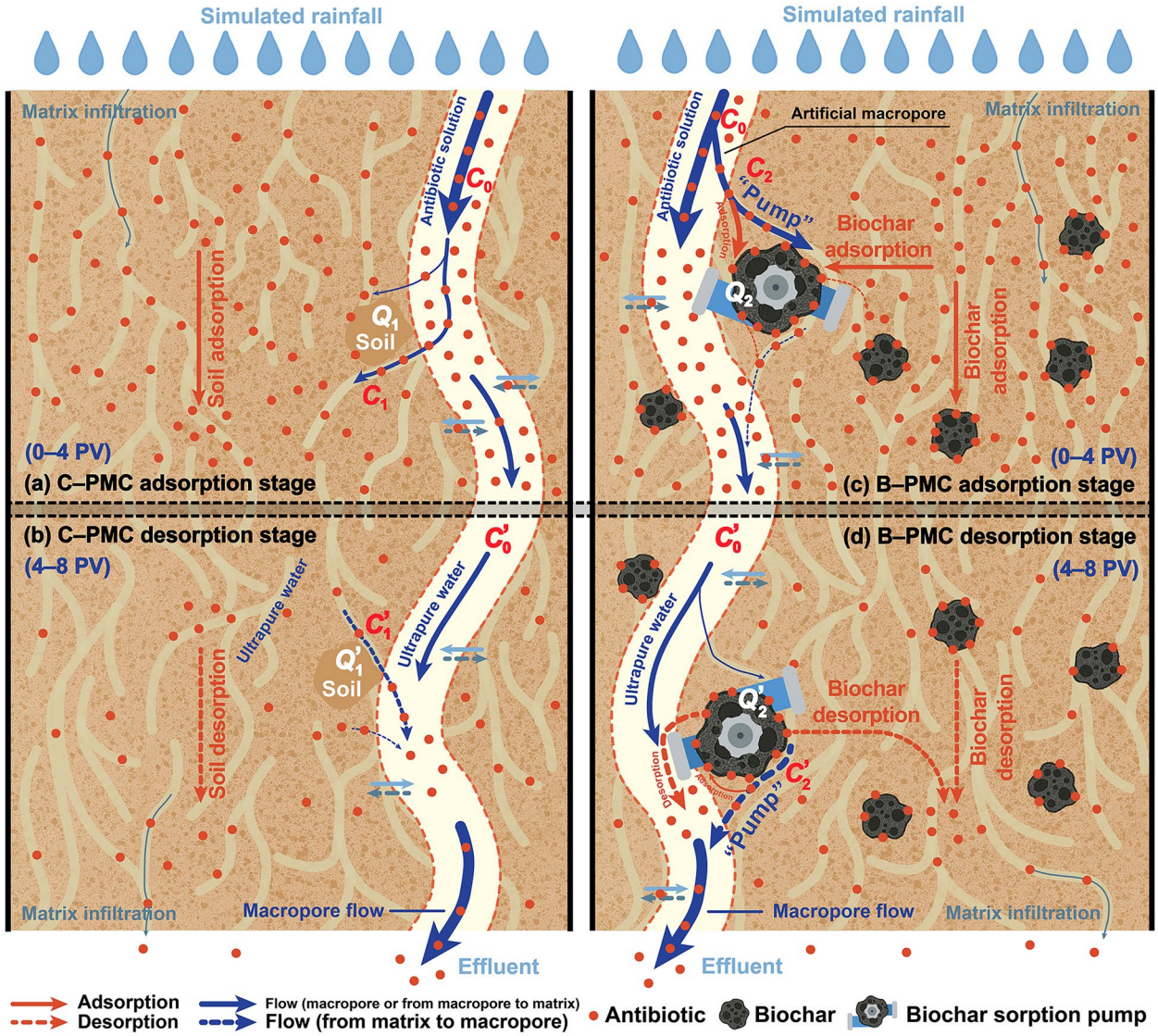

Fig. 7 The "biochar sorption pump" (BSP) hypothesis for enhanced antibiotic sequestration in a permeable dual-domain soil. This conceptual model illustrates the distinct processes during the adsorption (**a**, **c**) and desorption (**b**, **d**) stages in both control (**a**, **b**) and biochar-amended (**c**, **d**) treatments. The BSP hypothesis is driven by the stark differences in sorption capacity (K_d) and hysteresis between soil particles and biochar. During the adsorption stage (0–4 PV), an influent antibiotic concentration (C_0) establishes a gradient. In control soil, sorption onto soil particles (Q_1) results in a matrix infiltration concentration (C_1), whereas in the biochar-amended treatment, high sorption onto biochar particles (Q_2) driven by a much higher K_d ($K_{d,biochar} \gg K_{d,soil}$) creates a powerful sink that maintains a lower matrix infiltration concentration ($C_2 \ll C_1$), actively pumping solutes from the macropore flow. Subsequently, during desorption (4–8 PV), flushing with clean water (C_0') reverses this dynamic. While solutes readily desorb from soil particles (Q_1'), biochar's strong hysteretic binding minimizes solute release ($Q_2' \ll Q_1'$), effectively locking in the sequestered antibiotics. The relationship between adsorbed (Q) and porewater (C) concentrations is governed by K_d via the equation $Q = K_d \cdot C$

pathways that can further enhance the long-term attenuation of antibiotics in field environments. The magnitude of this regulation is specific to the 1% (w/w) crop-residue biochar employed. Variations in feedstock, pyrolysis temperature, and dosage will inevitably alter physicochemical properties, thereby modulating the pump's efficiency. While this study focused on single-cycle mechanisms, our parallel long-term field monitoring confirms the BSP effect persists under complex wetting–drying conditions, though its efficiency is modulated by structural evolution (Liu et al. 2024; Tang et al. 2024).

5 Conclusion

This study provides a new conceptual framework for understanding and controlling antibiotic pollution driven by transport processes in structured soils. Under the specific

experimental conditions of 1% (w/w) biochar amendment, it experimentally showed that biochar's efficacy is not intrinsic but an emergent property of the soil–biochar system, dependent on hydraulic connectivity between macropore and matrix domains. When this interface is permeable, biochar acts as a dynamic regulator of contaminant transport, activating a "biochar sorption pump" (BSP). By establishing a steep interfacial gradient to partition contaminants, this process reduced total relative maximum cumulative mass fluxes, validating biochar as an active sink rather than a passive barrier. Crucially, this mechanism of flux partitioning provides a pivotal bridge, reconciling the persistent disconnect between sorption-dominated laboratory experiments and observations of dual-domain transport at the field scale. The BSP framework thus offers a predictive tool for optimizing in-situ remediation, enabling the strategic application of biochar based on a site's soil structural properties to maximize sequestration efficiency. While these findings establish a mechanistic baseline, the optimal parameters for the BSP effect must be tailored to specific biochar properties and soil conditions in practical remediation strategies. This work confirms the efficacy of this mechanism in a stable, field-aged biochar system, but further research is imperative to evaluate the universality of this regulation under diverse climatic scenarios and varying biogeochemical conditions. Future research should also prioritize validating these transport models under variable field conditions to further optimize biochar application strategies for practical contaminant remediation. Ultimately, these findings provide a robust scientific basis for developing more precise and resource-efficient management strategies to mitigate contaminant leaching in structured soils and protect vulnerable water resources globally.

Supplementary Information

The online version contains supplementary material available at https://doi.org/10.1007/s42773-026-00596-x.

Supplementary material 1

Author contributions

Xinyu Liu: Investigation, Writing–original draft, Writing–review & editing, Data curation, Formal analysis, Validation. Yang He: Funding acquisition, Methodology, Investigation, Conceptualization, Validation, Writing–review & editing, Supervision. Jinghan Li: Investigation, Data curation, Software. Shijie Zheng: Investigation, Data curation, Software. Lei Zhang: Investigation, Data curation. Jianqiang Zhang: Funding acquisition, Supervision. Xiangyu Tang: Conceptualization, Funding acquisition, Resources.

Funding

This work was supported by the Sichuan Science and Technology Program (2026NSFSC0270), the China Postdoctoral Science Foundation (2025M782503), the Fundamental Research Funds for the Central Public-interest Scientific Institution (2024YSKY-05), the Open Research Fund of Key Laboratory of Eco-industry of Ministry of Ecology and Environment, Chinese Research Academy of Environmental Sciences (2024KFF-04), and the Key Research, Development Program of Ganzi Prefecture's Science and Technology Plan (24kjjh0005).

Data availability

The datasets used or analyzed during the current study are available from the corresponding author upon reasonable request.

Declarations

Competing interests

All authors certify that they have no affiliations with or involvement in any organization or entity with any financial interest or non-financial interest in the subject matter or materials discussed in this manuscript.

Author details

[1]School of Environmental Science and Engineering, Southwest Jiaotong University, Chengdu 611756, China. [2]Key Laboratory of Mountain Surface Processes and Ecological Regulation, Institute of Mountain Hazards and Environment, Chinese Academy of Sciences, Chengdu 610299, China. [3]Sichuan Yanting Agro-Ecosystem Research Station in Chinese National Ecosystem Research Network (CERN), Mianyang 621600, China. [4]Sichuan Engineering Research Center for Pollution Control in Rail Transit Engineering, Chengdu 611756, China. [5]Sichuan International Science and Technology Cooperation Base for Intelligent Environmental Protection and Sustainable Development in Rail Transit, Chengdu 611756, China. [6]National Key Laboratory for Development and Utilization of Forest Food Resources, College of Forestry and Biotechnology, Zhejiang A&F University, Hangzhou 311300, China.

Received: 23 October 2025 Revised: 2 February 2026 Accepted: 11 February 2026
Published online: 27 March 2026

References

Cao Y, Zhang K, Liu S, Wang Y (2024) A review of advancements in the theory and characterization of soil macropore structure. PeerJ 12:e18442. https://doi.org/10.7717/peerj.18442

Chen Y, Zwieten LV, Xiao K, Liang C, Ren J, Zhang A, Li Y, Dong H, Sun K (2024) Biochar as a green solution to drive the soil carbon pump. Carbon Res 3:44. https://doi.org/10.1007/s44246-024-00132-1

Dong S, Zhou M, Su X, Xia J, Wang L, Wu H, Suakollie EB, Wang D (2022) Transport and retention patterns of fragmental microplastics in saturated and unsaturated porous media: a real-time pore-scale visualization. Water Res 214:118195. https://doi.org/10.1016/j.watres.2022.118195

Du Y, Guo S, Wang R, Song X, Ju X (2023) Soil pore structure mediates the effects of soil oxygen on the dynamics of greenhouse gases during wetting–drying phases. Sci Total Environ 895:165192. https://doi.org/10.1016/j.scitotenv.2023.165192

Engelhardt I, Sittig S, Šimůnek J, Groeneweg J, Pütz T, Vereecken H (2015) Fate of the antibiotic sulfadiazine in natural soils: experimental and numerical investigations. J Contam Hydrol 177–178:30–42. https://doi.org/10.1016/j.jconhyd.2015.02.006

Hair JF, Sabol MA (2025) Partial least squares structural equation modeling (PLS-SEM): a rapidly emerging SEM alternative. International encyclopedia of statistical science. Springer, Berlin, Heidelberg, pp 1880–1882. https://doi.org/10.1007/978-3-662-69359-9_466

He Y, Liu C, Tang XY, Xian QS, Zhang JQ, Guan Z (2019) Biochar impacts on sorption-desorption of oxytetracycline and florfenicol in an alkaline farmland soil as affected by field ageing. Sci Total Environ 671:928–936. https://doi.org/10.1016/j.scitotenv.2019.03.414

He Y, Zheng S, Li J, Zhang J (2022) An experimental device for studying macropore flow in soil. CN 217878795 U.

Hou D, Jia X, Wang L, McGrath SP, Zhu YG, Hu Q, Zhao FJ, Bank MS, O'Connor D, Nriagu J (2025) Global soil pollution by toxic metals threatens agriculture and human health. Science. 388:316–321. https://doi.org/10.1126/science.adr5214

Hu JS, Xiao HY, Tang XY, Yan H, Chen Z, Cheng JH, Li XY (2025) Polarity and fluorescent fractions of manure dissolved organic matter could affect differently the adsorption and desorption of antibiotics in soils. J Environ Manage 378:124767. https://doi.org/10.1016/j.jenvman.2025.124767

Huan X, Zhang R, Qian J, Ma L, Fang Y, Yan Y (2024) Introducing a transition domain for describing the solute exchange between macropores/fractures and matrix in dual-permeability system. J Hydrol 634:131130. https://doi.org/10.1016/j.jhydrol.2024.131130

Ivanova N, Obaeed GLO, Sulkarnaev F, Buchkina N, Gubin A, Yurtaev A (2023) Effect of biochar aging in agricultural soil on its wetting properties and surface structure. Biochar 5:75. https://doi.org/10.1007/s42773-023-00272-4

Jia M, Lapen DR, Su D, Mayer KU (2023) Modeling of dual-permeability gas and solute reactive transport in macroporous agricultural soils with a focus on GHG cycling and emissions. J Hydrol 620:129408. https://doi.org/10.1016/j.jhydrol.2023.129408

Jiang Y, Zhang Y, Fan B, Wen J, Liu H, Mello CR, Cui J, Yuan C, Guo L (2023) Preferential flow influences the temporal stability of soil moisture in a headwater catchment. Geoderma 437:116590. https://doi.org/10.1016/j.geoderma.2023.116590

Jiao N, Luo T, Chen Q, Zhao Z, Xiao X, Liu J, Jian Z, Xie S, Thomas H, Herndl GJ, Benner R, Gonsior M, Chen F, Cai WJ, Robinson C (2024) The microbial carbon pump and climate change. Nat Rev Microbiol 22:408–419. https://doi.org/10.1038/s41579-024-01018-0

Lei W, Tang X, Zhou X (2020) Biochar amendment effectively reduces the transport of 3,5,6-trichloro-2-pyridinol (a main degradation product of chlorpyrifos) in purple soil: experimental and modeling. Chemosphere 245:125651. https://doi.org/10.1016/j.chemosphere.2019.125651

Li Z, Zhang X, Wang D, Liu Y (2018) Direct methods to calculate the mass exchange between solutes inside and outside aggregates in macroscopic model for solute transport in aggregated soil. Geoderma 320:126–135. https://doi.org/10.1016/j.geoderma.2018.01.021

Li H, Hu J, Yao L, Shen Q, An L, Wang X (2020a) Ultrahigh adsorbability towards different antibiotic residues on fore-modified self-functionalized biochar: competitive adsorption and mechanism studies. J Hazard Mater 390:122127. https://doi.org/10.1016/j.jhazmat.2020.122127

Li X, Wen Z, Zhu Q, Jakada H (2020b) A mobile-immobile model for reactive solute transport in a radial two-zone confined aquifer. J Hydrol 580:124347. https://doi.org/10.1016/j.jhydrol.2019.124347

Li Z, Kravchenko AN, Cupples A, Guber AK, Kuzyakov Y, Philip Robertson G, Blagodatskaya E (2024) Composition and metabolism of microbial communities in soil pores. Nat Commun 15:3578. https://doi.org/10.1038/s41467-024-47755-x

Liang C, Schimel JP, Jastrow JD (2017) The importance of anabolism in microbial control over soil carbon storage. Nat Microbiol 2:17105. https://doi.org/10.1038/nmicrobiol.2017.105

Lin H (2022) How do soil organic carbon pool, stock and their stability respond to crop residue incorporation in subtropical calcareous agricultural soils? Agric Ecosyst Environ 332:107927. https://doi.org/10.1016/j.agee.2022.107927

Liu C, Wang H, Li P, Xian Q, Tang X (2019a) Biochar's impact on dissolved organic matter (DOM) export from a cropland soil during natural rainfalls. Sci Total Environ 650:1988–1995. https://doi.org/10.1016/j.scitotenv.2018.09.356

Liu CH, Chuang YH, Li H, Boyd SA, Teppen BJ, Gonzalez JM, Johnston CT, Lehmann J, Zhang W (2019b) Long-term sorption of lincomycin to biochars: the intertwined roles of pore diffusion and dissolved organic carbon. Water Res 161:108–118. https://doi.org/10.1016/j.watres.2019.06.006

Liu Z, Ogunmokun FA, Wallach R (2022) Does biochar affect soil wettability and flow pattern? Geoderma 417:115826. https://doi.org/10.1016/j.geoderma.2022.115826

Liu XY, Gu XY, Liu C, Gbadegesin LA, He Y, Zhang JQ (2024) Field migration of veterinary antibiotics via surface runoff from chicken-raising orchard in responding to natural rainfalls. Sci Total Environ 909:168527. https://doi.org/10.1016/j.scitotenv.2023.168527

Liu X, He Y, Li J, Li J, Zhang J, Tang X (2025a) Does biochar field aging reduce the kinetic retention for weakly hydrophobic antibiotics in purple soil? Biochar 7:69. https://doi.org/10.1007/s42773-025-00460-4

Liu X, He Y, Zhang L, Xia L, Song W, Zhang J, Ouyang F (2025b) Experimental and modeling insights into adsorption and leaching of sulfadiazine and florfenicol in saturated porous media: role of multiple wet-dry cycling aged biochar. J Soils Sediments 25:1911–1926. https://doi.org/10.1007/s11368-025-04048-0

Liu XY, Gbadegesin LA, He Y, Zhang JQ, Liu C (2025c) Plot-scale observation on antibiotics migration in surface runoff and leachate from chicken-raising orchard of Entisol during rainstorms. Ecotoxicol Environ Saf 294:118105. https://doi.org/10.1016/j.ecoenv.2025.118105

Lu J, Luo Y, Huang J, Hou B, Wang B, Ogino K, Zhao J, Si H (2023) Evaluating the effects of biochar on the hydraulic properties of acidified soil in China. J Soils Sediments 23:223–231. https://doi.org/10.1007/s11368-022-03327-4

Manns HR, Jiang Y, Parkin G (2024) Soil pores in preferential flow terminology and permeability equations. Vadose Zone J 23:e20365. https://doi.org/10.1002/vzj2.20365

Mason CH, Perreault WD (1991) Collinearity, power, and interpretation of multiple regression analysis. J Mark Res 28:268. https://doi.org/10.2307/3172863

McCarter CPR, Rezanezhad F, Quinton WL, Gharedaghloo B, Lennartz B, Price J, Connon R, Van Cappellen P (2020) Pore-scale controls on hydrological and geochemical processes in peat: implications on interacting processes. Earth-Sci Rev 207:103227. https://doi.org/10.1016/j.earscirev.2020.103227

Miele F, Benettin P, Wang S, Retti I, Asadollahi M, Frutschi M, Mohanty B, Bernier-Latmani R, Rinaldo A (2023) Spatially explicit linkages between redox potential cycles and soil moisture fluctuations. Water Resour Res 59:e2022WR032328. https://doi.org/10.1029/2022WR032328

Pollacco JAP, Eger A, Rajanayaka C, Fernández-Gálvez J (2024) Improved partitioning between matrix and macropore flow: novel bimodal lognormal functions for water retention and hydraulic conductivity in pumice and non-pumice soils. J Hydrol 644:131985. https://doi.org/10.1016/j.jhydrol.2024.131985

Radolinski J, Pangle L, Klaus J, Stewart RD (2021) Testing the 'two water worlds' hypothesis under variable preferential flow conditions. Hydrol Process 35:e14252. https://doi.org/10.1002/hyp.14252

Sharma A, Swami D, Joshi N, Chandel A, Šimůnek J (2021) The semi-analytical solution for non-equilibrium solute transport in dual-permeability porous media. Water Resour Res 57:e2020WR029370. https://doi.org/10.1029/2020wr029370

Silva LPD, Van Lier QDJ, Correa MM, Miranda JHD, Oliveira LAD (2016) Retention and solute transport properties in disturbed and undisturbed soil samples. Rev Bras Ciênc Solo 40:e0151045. https://doi.org/10.1590/18069657rbcs20151045

Souza R, Ghannam K, Calabrese S (2024) Dynamic coupling between soil properties and water content in shrink-swell soils: effects on surface hydrologic partitioning. Adv Water Resour 184:104630. https://doi.org/10.1016/j.advwatres.2024.104630

Srinivasan P, Sarmah AK (2015) Characterisation of agricultural waste-derived biochars and their sorption potential for sulfamethoxazole in pasture soil: a spectroscopic investigation. Sci Total Environ 502:471–480. https://doi.org/10.1016/j.scitotenv.2014.09.048

Tang XY, Yin WM, Yang G, Cui JF, Cheng JH, Yang F, Li XY, Wu CY, Zhu SG (2024) Biochar reduces antibiotic transport by altering soil hydrology and enhancing antibiotic sorption. J Hazard Mater 472:134468. https://doi.org/10.1016/j.jhazmat.2024.134468

Urbina CAF, Van Dam JC, Hendriks RFA, Van Den Berg F, Gooren HPA, Ritsema CJ (2019) Water flow in soils with heterogeneous macropore geometries. Vadose Zone J 18:1–17. https://doi.org/10.2136/vzj2019.02.0015

Wang J (2025) Addition of bacterial-feeding nematodes contributes to soil phosphorus availability by affecting the mineralization of moderately labile organic phosphorus. Appl Soil Ecol 205:105764. https://doi.org/10.1016/j.apsoil.2024.105764

Xian Q, Li P, Liu C, Cui J, Guan Z, Tang X (2018) Concentration and spectroscopic characteristics of DOM in surface runoff and fracture flow in a cropland plot of a loamy soil. Sci Total Environ 622–623:385–393. https://doi.org/10.1016/j.scitotenv.2017.12.010

Yu X, Wu C, Fu Y, Brookes PC, Lu S (2016) Three-dimensional pore structure and carbon distribution of macroaggregates in biochar-amended soil. Eur J Soil Sci 67:109–120. https://doi.org/10.1111/ejss.12305

Zhang L, Liu X, Li J, Zhu Y, Xiao Y, Zhang J, He Y (2025) Weakly hydrophobic antibiotics leaching in an alpine soil of the Tibetan Plateau in responding to macropore flow. J Hazard Mater 497:139774. https://doi.org/10.1016/j.jhazmat.2025.139774

Zou Y, Zheng W (2013) Modeling manure colloid-facilitated transport of the weakly hydrophobic antibiotic florfenicol in saturated soil columns. Environ Sci Technol 47:5185–5192. https://doi.org/10.1021/es400624w